PAPER

Check for updates

Integrated microfluidic platform based on potentiometric Sonogel-Carbon sensors for the simultaneous determination of Na+ and K+ in untreated human plasma and serum

Álvaro Jesús Sainz-Calvo, Álvaro Cordero-Hernández, Marina Jiménez-Rodríguez, [iD] Virginia García-Rodríguez, Juan José García-Guzmán,* Dolores Bellido-Milla,* José María Palacios-Santander [iD] and Laura Cubillana-Aguilera [iD]

In the present work, two potentiometric sensors for the simultaneous determination of sodium and potassium ions were successfully developed. A novel functionalized multi-walled carbon nanotube sonogel-based mixture served as ion-to-electron transducer, while sodium and potassium cocktail membranes were employed as ion-selective membranes. Both sensors exhibit a well-defined operational range suitable for the precise quantification of these cations in the biomedical range, the sensors showed linear ranges of 38–4400 and 0.31–314 mM for sodium and potassium, respectively. The LOD and LOQ were 0.28/0.31 mM and 0.38/0.64 mM, respectively while the sensitivities were 58.3 ± 0.5 and 54 ± 0.2 mV per decade. The sensors demonstrate outstanding repeatability, reproducibility, and reversibility, with relative standard deviations (% RSD) below 5%, as well as exceptional selectivity for Na+ and K+ ions in the presence of various interferent substances commonly found in biological matrices. Furthermore, the sensors were applied for the simultaneous determination of sodium and potassium in untreated human plasma and serum samples under continuous flow conditions using a microfluidic cell, whose fabrication is really simple using 3D printing and cost of fabrication is less than 1 euro, and requiring only a minimal sample volume (~300 µL). The analytical results obtained showed an error margin of less than 5% across all tested samples, highlighting the sensor's reliability and potential applicability in clinical diagnostics. Notably, an excellent correlation was observed with the reference technique routinely employed in hospitals, the blood gas analyser, further supporting clinical relevance of the sensors. These findings underscore the practical utility of the developed sensors for rapid and accurate ion monitoring in complex biological fluids.

1. Introduction

In the medicine field, public health represents a fundamental pillar whose relevance extends beyond the clinical domain encompassing a population wide-health.[1,2] Most public healthcare systems face substantial challenges, such as prolonged waiting times in emergency services to access primary care.[3] Early disease detection is, therefore, essential to ensure effective treatment, improve patients' quality of life, and reduce the burden on healthcare professionals.[4]

Digital technologies have become increasingly important in addressing these challenges by enabling improved communication, health monitoring, and access to medical information, contributing to the sustainability of healthcare systems.[5] This has led to the emergence of electronic Health (e-Health), defined by the World Health Organization (WHO) as "the use of digital information, transmitted, stored, or retrieved electronically, in the health sector to support health care at both local and remote levels".[6] Today, e-Health applications allow for remote monitoring, diagnostics, and the provision of rapid and effective assistance for all users.[7,8]

In this context, wearable and miniaturized sensors have gained increasing attention due to their ability to provide continuous, real-time monitoring of clinically relevant

Institute of Research on Electron Microscopy and Materials (IMEYMAT), Department of Analytical Chemistry, Faculty of Sciences, Campus de Excelencia Internacional del Mar (CEIMAR), University of Cadiz, Campus Universitario de Puerto Real, Polígono del Río San Pedro S/N, Puerto Real, 11510 Cádiz, Spain. E-mail: alvarojesus.sainz@uca.es, alvaro.corderohernandez@alum.uca.es, marina.jimenezrodriguez@alum.uca.es, virginia.garciarodriguez@alum.uca.es, juanjo.garciaguzman@uca.es, dolores.milla@uca.es, laura.cubillana@uca.es, josem.palacios@uca.es

parameters such as glucose, urea, lactate, cholesterol, and electrolytes, including sodium, potassium, calcium, and magnesium.[9–12] The integration of biosensors into clinical practice enables real-time data transmission to healthcare professionals, improving patient care while enhancing accessibility, convenience, and analytical accuracy.[13]

Among electrolytes, sodium and potassium are two highly informative biomarkers for evaluating a patient's health status.[14,15] Both ions play essential roles in numerous physiological processes, and even minor deviations from their normal concentration ranges can indicate serious health conditions.[16,17] Typical reference values range from 3.5 to 5.2 mM for potassium[15] and from 135 to 145 mM for sodium.[18] Alterations in potassium levels are associated with cardiovascular and neurological disorders, including hypertension and stroke,[19] whereas sodium imbalances are closely linked to kidney dysfunction and fluid regulation disorders.[16] Importantly, many physiological processes rely on the finely regulated balance between sodium and potassium, particularly through the Na^+/K^+-ATPase, which is essential for maintaining cellular homeostasis, nerve impulse propagation, and muscle contraction.[20–22] These considerations highlight the clinical relevance of their simultaneous determination.

Conventional analytical techniques for sodium and potassium determination include spectroscopic methods, such as flame atomic emission spectroscopy and inductively coupled plasma (ICP) techniques.[23,24] Although highly precise and sensitive, these approaches require extensive sample preparation, expensive instrumentation, and highly trained personnel, limiting their applicability for routine analysis and point-of-care testing (POCT).[25–27]

In contrast, electroanalytical techniques based on ion-selective electrodes (ISEs) offer significant advantages.[28,29] Potentiometric methods are characterized by their speed, simplicity, and the ability to perform direct determination of sodium and potassium in several matrices, including biological samples, with minimal or no sample treatment.[30] The immediacy and ease of use allow for the direct measurement of ionic activity without additional sample preparation. Moreover, electroanalytical systems are more portable and economical, supporting the development of in situ and POCT devices.[31] While these methods have yielded reliable results in previous studies,[32–34] few focus on the simultaneous detection of both ions. A recent study successfully demonstrated the simultaneous detection of sodium, potassium, and calcium in sweat samples, a relatively simple matrix.[35] Other sensors applied to biomedical samples have been also reported,[36–38,42] but many rely on expensive or less accessible transducer materials, like structured silicon nanowire or modified carbon paste whose fabrication is very complex,[39,40] have limited long-term stability or show reduced biocompatibility,[37–41] hindering their practical use in continuous monitoring applications.

The development of robust potentiometric sensors for complex biomedical matrices remains a significant analytical challenge due to the strict requirements for potential stability, low detection limits, and long-term reproducibility.[43,65–67] In this regard, carbon nanotubes (CNTs) have emerged as highly efficient ion-to-electron transducers, offering high electrical conductivity, large double-layer capacitance, and chemical stability, which provide stable potential signals and minimize drift under continuous flow conditions.[42,65]

While previous studies have incorporated multiwalled carbon nanotubes into carbon paste transducers,[46] the present work develops a ceramic composite by incorporating functionalized MWCNTs into a sonogel matrix using an ultrasound-assisted procedure. This method enables rapid, homogeneous, and reproducible dispersion of the nanotubes,[42] overcoming limitations associated with traditional alcoholic dispersions, which are often slow and prone to re-aggregation.[68–72] The resulting composite exhibits excellent nanostructural integration, chemical resilience, and mechanical stability, enhancing the reproducibility and performance of the electrodes. To the best of our knowledge, this synthetic route has not been previously reported and represents a novel and environmentally friendly strategy for producing CNT-modified sol–gel materials. This approach may facilitate the fabrication and application of potentiometric sensors by enabling the use of easily, accessible components and cost-effective fabrication procedures, as well as their integration into platforms for continuous-flow analysis of biomedical samples.

In this paper, authors report the development of a low-cost, miniaturized potentiometric platform based on Sonogel-Carbon electrodes for the simultaneous determination of sodium and potassium in untreated human serum and plasma under continuous-flow conditions. The novelty of this paper is the development of a system which combines a tandem of ion-selective membranes with a sonogel–f-MWCNTs ion-electron transducer, enabling real-time monitoring. Besides, the multianalyte device is fabricated using 3D printing, allowing rapid, reproducible, and highly economical production (under 1 euro per unit). Thus, this piece of research proposes a system to overcome limitations of previous work, which mostly relied on simple matrices such as sweat or saliva, expensive transducer materials, or complex fabrication procedures.[35–41] Overall, the analytical platform demonstrates robust, reproducible, and selective detection of clinically relevant ions, offering a practical, sustainable, and scalable solution for point-of-care testing and clinical diagnostics in complex biological matrices.

2. Materials and methods

2.1 Reagents

Bis(2-ethylhexyl) sebacate (DOS), 4-tertiarybutylalkylix arene tetraethyl tetraester tetraethyl acid (sodium ionophore X), sodium tetrakis[3,5-bis(trifluoromethyl)phenyl]borate (Na-TFPB), potassium ionophere I (valinomycin), polyurethane (PU),

tetrahydrofuran (THF), lithium perchlorate and polyvinyl butyral (PVB) were obtained from Sigma-Aldrich (St. Gallen, Switzerland). Potassium tetrakis (4-chloropentyl) borate and graphite powder were obtained from Thermo Scientific (Kandel, Germany). Hydrochloric acid, orthophosphoric acid, potassium hydroxide, sodium, potassium, calcium, and magnesium chloride, D-(+)-glucose anhydrous, and urea were purchased from PanReac (Castellar des Vallàs, Barcelona, Spain). Methyltrimethoxysilane (MTMOS), boric acid, ammonium chloride, and bovine serum albumin (BSA) were purchased from Merck (Darmstadt, Germany). Multi-walled carbon nanotubes functionalised with carboxylic groups (MWCNT-COOH) were obtained from DropSens-Metrohm (Asturias, Spain). Di-potassium hydrogen phosphate and potassium dihydrogen phosphate were obtained from Labkem (Premià de Dalt, Barcelona, Spain). Glacial acetic acid was purchased from GlobalChem (Sevilla, Spain). Glass capillary tubes (i.d. 1.23 mm, 0.05 mm) were used as the bodies of the electrodes. All the solutions were prepared with nanopure water (18 MΩ cm) from the Wasser Lab Ultramic Plus (Type I) system (Barbatáin, Spain).

2.2 Instrumentation

A high-energy ultrasound probe was used in the synthesis of the electrodes using a MISONIX S-400 ultrasonic generator (New York, NY, USA) coupled with a 13 mm diameter titanium tip. All electrochemical tests were performed using an Autolab PGSTAT 12 from EcoChemie (Herisau, Switzerland) and a μStat 8000-portable multichannel potentiostat/galvanostat from DropSens-Metrohm (Asturias, Spain). The electrodeposition experiments were performed in a cell composed of three electrodes at room temperature. A modified Sonogel-Carbon electrode was used as the working electrode, Ag/AgCl (KCl 3 M) as the reference electrode, and a platinum rod as the counter electrode. The pH-meter GLP21 (Crison from Barcelona, Spain) was used in the preparation of the Britton–Robinson (BR) and phosphate buffer saline (PBS) solutions.

The software FreeCAD 0.20 was used to design a 3D microfluidic cell, whereas the software PrusaSlicer 2.6.1 was used to export the model and print the data. The fabrication of the cell was performed with a 3D printer Original Prusa MINI+ (Praga, Czech Republic) using filaments of polyethylene terephthalate glycol (PETG) from Prusa (Praga, Chez Republic). A peristaltic pump Minipuls 2 from Gilson (Middleton, WI, USA) was used for continuous flow regime measurements.

A gas analyzer named GEM® CVP 2 provided by Instrumental Laboratory Company (Bedford, USA) was used as a reference technique for validation purposes.

2.3 Preparation and conditioning of Sonogel-Carbon electrodes and multiwalled carbon nanotubes

The preparation of the Sonogel-Carbon (SNG-C) electrodes has been previously described in the literature.[44,45] Briefly, 500 μL of MTMOS and 100 μL of HCl 0.2 M are mixed and

sonicated for 10 s at 40% amplitude using a high-energy ultrasound probe. Subsequently, 500 mg of graphite is added and thoroughly mixed to produce a uniform paste. Finally, glass capillary tubes are filled with the resulting paste, and after 24 hours of drying, the electrodes are gently polished with P1200 emery paper (Struers, Germany).

Before their use, the SNG-C electrodes were conditioned in PBS (0.1 M) buffer solution. This step was carried out by performing 5 scans in cyclic voltammetry, in the potential range from −1 to 1 V at 50 mV s^{-1}.

In order to carry out the preparation of the f-MWCNT-based sol–gel composite, the synthesis of the carbon nanotube composite material was performed as follows: 500 μL of methyltrimethoxysilane (MTMOS) is combined with 100 μL of 0.6 M hydrochloric acid, which acts as a catalytic agent. The resulting mixture is subjected to sonication for 10 seconds at 40% amplitude using a high-energy ultrasonic probe. Subsequently, 23.5 mg of functionalized multi-walled carbon nanotubes (f-MWCNTs) are incorporated and thoroughly homogenized to obtain a uniform liquid dispersion (sonogel–f-MWCNTs) (Fig. 1 and S1A).

2.4 Fabrication of the potassium and sodium membrane

The fabrication of both potassium and sodium ion-selective membranes was carried out following previously reported methodologies with minor modifications, as described in references.[47,48] In each case, approximately 32.8 mg of polyurethane was dissolved in 1 mL of tetrahydrofuran (THF) in a sealed vial. To ensure complete dissolution, the mixture was placed in an ultrasonic bath for approximately 4 hours, with periodic vortex mixing and careful temperature control to avoid THF evaporation and polymer degradation. In parallel, the ion-selective components were prepared in separate vials. For the potassium-selective membrane, 0.5 mg of potassium tetrakis(4-chlorophenyl)borate (KTClPB), 2 mg of potassium ionophore I (valinomycin), and 647 μL of bis(2-ethylhexyl) sebacate (DOS) were used. For the sodium-
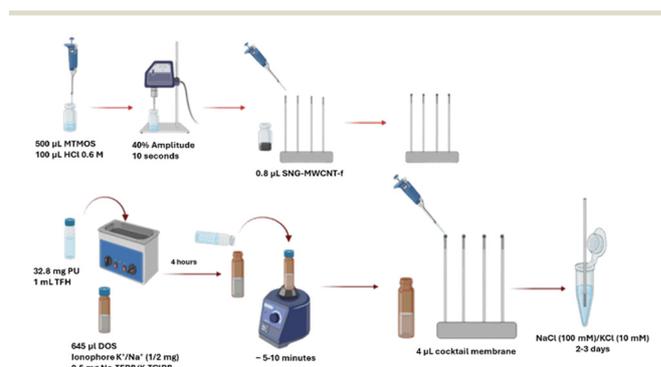

Fig. 1 Schematic representation of the fabrication process of the sonogel-functionalized carbon nanotubes (SNG-f-MWCNTs) composite, the preparation of the sodium and potassium ion-selective membrane cocktails, and the assembly of the corresponding sodium and potassium chemical sensors. More information can be found in the SI section, Fig. S1A–C.

selective membrane, the corresponding mixture contained 0.5 mg of tetrakis[3,5-bis(trifluoromethyl)phenyl]sodium borate (Na-TFPB), 1 mg of sodium ionophore X, and 645 μL of DOS. After the polyurethane solution was fully dissolved, 1 mL was added to the respective ionophore/plasticizer mixture and homogenized thoroughly using vortex agitation to obtain the final membrane cocktails (Fig. 1 and S1B and C). Due to the volatility of THF, the resulting solutions were stored in tightly sealed vials, wrapped in Parafilm, and kept at 4 °C for no longer than two weeks.

2.5 Fabrication of potassium and sodium ion selective electrodes

The fabrication process of the potentiometric sodium and potassium sensors begins with the deposition of the ion-to-electron transducer layer, composed of multi-walled carbon nanotubes-functionalized sol–gel composite material, onto the surface of the SNG-C electrodes. Since a membrane cocktail is subsequently applied, it is crucial to minimize the deposited volume while ensuring uniform coverage of the electrode surface. This approach prevents the formation of surface irregularities that could compromise the adhesion and performance of the membrane layer and avoids undesired water filtration. Employing a drop-casting technique with a micropipette, the optimal deposition volume was determined to be 0.8 μL, and the sample was left to dry at room temperature for 24 hours. 4 μL of the membrane cocktail was deposited in order to completely cover the electrode and ensure proper coating. This volume was deemed the most appropriate, as it is expected to enhance the sensor sensitivity. This membrane cocktail was applied to the electrode surface by drop-casting using a micropipette. The deposited membrane was allowed to dry 12–24 hours to facilitate solvent evaporation and promote maximum homogenization of the membrane components. Subsequently, the sensors were conditioned by immersion in solutions for 2–3 days: sodium-selective electrodes were immersed in a 100 mM Na^+ solution, while potassium-selective electrodes were conditioned in a 10 mM K^+ solution.[47]

2.6 Calibration and figure of merits

To study the behaviour of the sensor in a wide range containing regular and abnormal concentrations of Na^+ and K^+, different standard solutions were prepared, whose solvents were PBS for Na^+ and BR buffer for K^+. For the construction of the calibration curve, a series of NaCl standard solutions with known sodium activities was prepared, varying from −1.5 to 1 ($\log a_{Na^+}$ = −1.5, −1, −0.5, 0, 0.5 and 1), with the activity of the ion increasing in steps of 0.5 units. In the case of potassium, the calibration was conducted in the activity range from −3.26 to −1 ($\log a_{K^+}$ = −3.26, −2.80, −2.35, −1.90, −1.45, and −1.00).

Repeatability, reproducibility, reversibility, signal stability, limit of detection, and limit of quantification were assessed.

Besides, selectivity was studied using the Separate Solution Method (SSM), which evaluates the sensor's ability to distinguish the target analyte from potential interfering substances.[49] For each interferent, three calibration curves are constructed using standard solutions with concentrations that encompass the typical levels found in biological samples. Additionally, a calibration curve is prepared using potassium and sodium standards. The interfering substances studied include Li^+, NH_4^+, Na^+, K^+, Ca^{2+}, Mg^{2+}, phosphates such as K_2HPO_4 and Na_2HPO_4, glucose, urea, and bovine serum albumin (BSA). It is important to note that the selection of interferents depends on the electrode employed: for the sodium-selective electrode, K^+ and K_2HPO_4 are evaluated as interferents, while for the potassium-selective electrode, Na^+ and Na_2HPO_4 are considered as potential interferents.

2.7 Fabrication of the pseudoreference Ag/AgCl electrode

A pseudoreference Ag/AgCl electrode was fabricated following a previously described procedure.[50] In brief, a silver rod was polished and immersed in a 0.1 mg mL^{-1} AgCl solution for 48 hours, ensuring the process was carried out in the absence of light. After this time, the electrode was coated with multiple layers of polymer. First, the AgCl-modified silver rod was coated with three 0.3 μL layers of a polyvinyl butyral (PVB) solution, prepared with 74.8 mg L^{-1} of PVB and 50 mg mL^{-1} of NaCl dissolved in 1 mL of methanol. Following this, a single 0.3 μL layer of polyurethane (PU) solution, consisting of 30 mg mL^{-1} of PU in 1 mL of tetrahydrofuran, was applied. Once the coating process was complete, the pseudoreference electrode was stored in a cold environment for at least 24 hours, fully submerged in a KCl 3 M solution (please, see Fig. S2).

2.8 Simultaneous detection of sodium (Na^+) and potassium (K^+) ions in real samples using continuous flow mode

To improve the analytical efficiency and reduce sample consumption, the ion-selective electrodes were integrated into a continuous flow microfluidic cell. This configuration allows real-time monitoring and enables both independent and simultaneous detection of Na^+ and K^+ ions in complex biological matrices, such as human plasma and serum.

The electrochemical cell for this purpose is based on the sodium and potassium sensors as the working electrode and a modified silver rod as the pseudo-reference electrode.

A three-dimensional microfluidic cell was designed using FreeCAD software specifically for the continuous operation of the sodium and potassium sensor. This cell was fabricated using an Original Prusa MINI+ 3D printer, employing polyethylene terephthalate glycol (PETG) as the polymeric filament.

Continuous measurements were performed using a peristaltic pump with a flow speed of 0.4 mL min^{-1}. Chronopotentiometric measurements were conducted under the following experimental conditions: the applied current

was set to 0 A, the total measurement time was about 3000 seconds, and data were recorded at 0.9 second intervals.

2.9 Real sample analysis and validation of the potentiometric sensors

For validation purposes, a calibration standard for gas analysers was used as a reference value. The sample was analysed without dilution or any additional treatment.

Human serum samples were collected by trained personnel from healthy adult volunteers at the University Hospital of Puerto Real (Cádiz, Spain). Serum was obtained by centrifuging the collected blood at 3500 rpm for 5 minutes using serum separator tubes (SST) containing a separation gel primarily composed of silicone, polyester, and synthetic oils. Plasma was obtained by centrifuging the blood samples at 3500 rpm for 10 minutes using tubes containing anticoagulants.

3. Results and discussion

3.1 Analytical performance of sodium (Na$^+$) and potassium (K$^+$) ion-selective electrodes

Once the chemical sensors have been properly conditioned, individual calibration is performed using several standard sodium and potassium solutions, as described in section 2.6. These solutions span a concentration range that includes both physiological levels, values slightly above and below those typically found in human blood, ensuring accurate response across clinically relevant conditions. During calibration, the electrode potential is measured and plotted against the logarithm of the ion activity ($\log a$) for the ion of interest. The resulting calibration curve should yield a linear relationship described by the equation $y = mx + n$, where m represents the slope and n the intercept. Ideally, the slope should closely approximate the Nernstian response, which

for monovalent ions is approximately 0.059 V per decade of activity at room temperature, as defined in eqn (1). This linearity and slope serve as indicators of proper sensor function and ion selectivity, both of which are essential for reliable analytical performance.

$$E = E_0 + 0.59 \log a_{M^{n+}} \tag{1}$$

In Fig. 2, the chronopotentiograms and the calibration curves for sodium and potassium sensors are shown. In the first one, the potentials recorded for each standard solution of the ion are distinguishable, showing clear and significant differences between the signals corresponding to the various concentrations of both ions. This differentiation enables a precise discrimination of the responses associated with each concentration level. Using the data obtained, calibration curves were constructed by plotting the measured potentials against the logarithm of the respective ion activities, which accounts for the non-ideal behaviour of ions in solution and thus provides a more accurate representation of the sensor performance. As shown in Fig. 2B, the calibration curve for sodium demonstrates a strong linear correlation, with a slope of 0.0583 V, which perfectly aligns with the theoretical value predicted by the Nernst equation (59 mV per decade at 25 °C). Similarly, the potassium calibration curve exhibits comparable linearity and sensitivity, confirming that the sensor effectively detects potassium ions. These calibration results indicate that the sensors offer a wide linear range and excellent reproducibility for both sodium and potassium ion measurements, like it has been reported in the literature such as appear in Table 1. Collectively, the data validate the sensor capability for selective, and reliable quantification of these biologically and environmentally important ions, demonstrating its potential for rapid analysis in complex matrices.
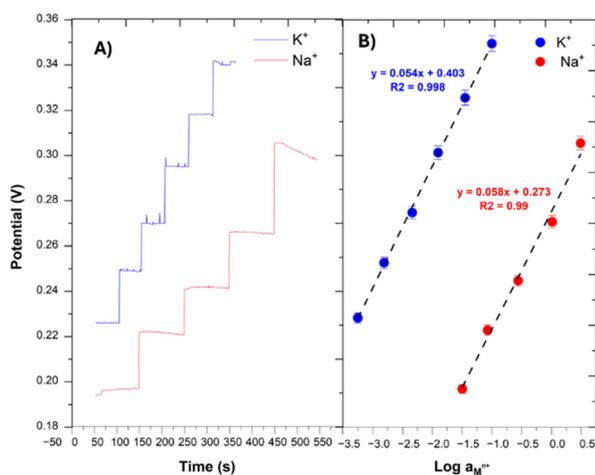
3.2 Figure of merits

3.2.1 Repeatability and reproducibility. To evaluate repeatability, a single sodium and potassium sensor was each subjected to four consecutive calibration cycles. In contrast, reproducibility was assessed by performing a single calibration on four independent sensors for each ion. In both cases, the calibration slope, understood as the sensitivity value, served as the primary performance metric. The repeatability obtained, expressed as relative standard deviation, was 0.99% for the sodium sensor and 1.45% for the potassium sensor. For reproducibility, the variability was 2.76% for the potassium sensor and 1.09% for the sodium sensor. All measurements complied with the ISO 5725-1:1994 standard,[59] confirming high repeatability and reproducibility, with all deviations remaining below the 5% deviation.

3.2.2 Limit of detection (LOD) and limit of quantification (LOQ). To ensure the quality and reliability of the proposed method, the limits of detection (LOD) and quantification (LOQ), see eqn (2), were determined for both sodium and

Fig. 2 Chronopotentiometric response and analytical performance of the sodium and potassium ion-selective electrodes operating in batch mode. (A) Chronopotentiograms recorded in PBS (0.1 M, pH 7.4) at different $\log a$ value of Na$^+$ and K$^+$. (B) Corresponding calibration curves ($n = 3$) derived from the potential-time data.

Table 1 Comprehensive comparison of the analytical performance of ion-selective membrane-based potentiometric sensors for sodium and potassium detection under controlled laboratory conditions

Sodium (Na⁺) potentiometric sensors

Na⁺ sensor	Concentration range (mM)	Slope (mV/log a_{Na^+})	Reference
3D-Na⁺	0.25–250	57.9	37
IKT-P-ISM(Na⁺)	0.1–100	62.5	58
GCE(CP)-SE-ISM(Na⁺)	0.21–24.54	58	51
CB-AuNPs-CH₃COOLi (L)-ISM(Na⁺)	1–1000	56.1	52
P_s-CNTs-ISM(Na⁺)	$1 \times 10^{-3} - 10$	59.08 ± 0.32	53
STM-CNTs-ISM(Na⁺)	0.1–100	54.1 ± 1.5	54
G/PEDOT:PSS-ISM(Na⁺)	0.1–1000	62.5 ± 2.1	55
SNG-C-CNTs-ISM(Na⁺)	38–4400	58.3 ± 0.5	This work

Potassium (K⁺) potentiometric sensors

K⁺ sensor	Concentration range (mM)	Slope (mV/log a_{K+})	Reference
MB-PDMS-CNTs-ISM(K⁺)	0.1–100	55.8 ± 0.6	55
PR-S-MWCNTs-ISM(K⁺)	50–120	55 ± 0.3	57
P_s-CNTs-ISM(K⁺)	0.1–100	59.15 ± 0.28	53
STM-CNTs-ISM(K⁺)	0.1–100	56.9 ± 1.5	54
G/PEDOT:PSS-ISM(K⁺)	0.1–1000	62.9 ± 1.1	56
IKT-P-ISM(K⁺)	0.1–100	62.9	58
SNG-C-CNTs-ISM(K⁺)	0.314–314	54 ± 0.2	This work

3D-Na⁺: 3D-printed Na⁺ sensor; GCE: glassy carbon electrodes; CP: carbon paste; CB: carbon black; AuNPs: gold nanoparticles; CH₃COOLi(L): layer of lithium acetate; IKT: inkjet printing impression; P_s: paper substrate; CNTs: carbon nanotubes; STM: stretchable material; G/PEDOT: PSS: graphene modified with poly(3,4-etilendioxitiophene)polystyrenesulfonate; MB: microneedle based ion selective electrode; PDMS: polydimethylsiloxane; PR-S: Parafilm substrate; ISM(K⁺): potassium ion selective membrane; ISM(Na⁺): sodium ion selective membrane.

potassium cations. The LOD and LOQ were calculated based on the standard deviation of the response and the slope of the calibration curve, using the following equations:

$$\text{LOD} = 3 \cdot \frac{\sigma}{s} \quad \text{and} \quad \text{LOQ} = 10 \cdot \frac{\sigma}{s} \qquad (2)$$

where σ is the standard deviation of the response and s is the slope of the calibration curve.

For sodium, the LOD was found to be 0.28 mM, while the LOQ was established at 0.38 mM. These values are significantly below the regular physiological concentration range of sodium in blood serum (135–145 mM), thereby allowing for accurate and broad-range quantification in real clinical samples. Similar determinations were carried out for potassium, yielding LOD and LOQ values of 0.31 and 0.64 Mm; these values are within the physiologically relevant concentration range. Consequently, the obtained limits of detection and quantification are adequate for practical applications in the medical field.

3.2.3 Reversibility, signal stability and lifetime. A reversibility experiment evaluated the sensor's ability to return to its initial state after multiple cycles of increasing and decreasing sodium and potassium concentrations (see Fig. 3). The plots showed consistent responses with no significant drift over successive calibrations when compared to the initial measurement (calibration 1), indicating excellent stability. Similar behaviour was observed for potassium, with comparable results. The chronopotentiograms closely resembled those reported for a potentiometric potassium sensor in the literature.[56]

Additionally, a statistical comparison between the slopes of the first and last calibration (both under increasing activities) yielded a coefficient of variation of 0.9% and 2.5% for sodium and potassium, respectively, both below the 5% threshold. These findings confirm the robustness of both sensors in reversibility and reliable performance under transient ion concentration conditions.

To evaluate the suitability of the sensor for long-term continuous measurements, a single chronopotentiometric
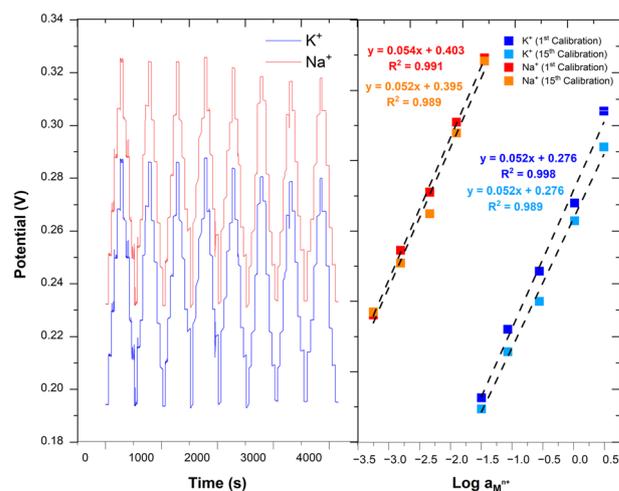

Fig. 3 Dynamic response and average calibrations for the hysteresis test (fifteen consecutive calibrations by alternative increasing and decreasing log a potassium and sodium standard solutions) carried out with the proposed potassium and sodium potentiometric sensors.

test was performed for several hours. A sodium and potassium standard solution with a fixed activity of $\log a$ = 1.07 and −2.38 for sodium and potassium, respectively, corresponding to a concentration of 110 mM in Na^+ and 4.17 mM in K^+, were used. These values were selected for its proximity to physiological sodium and potassium levels found in human serum.[60] These results, along with the stable signal, indicate no significant deviation over time. Statistical analysis further confirmed this stability, yielding a coefficient of variation of 0.96% and 0.8% for sodium and potassium, respectively.

Alternatively, assessing performance stability over time is essential for determining sensor lifespan. Since all fabricated electrodes have a limited operational life, a study was conducted to evaluate the sensor's long-term viability. For this purpose, calibration curves were recorded under consistent measurement conditions on several days following fabrication. The sensor sensitivity was tracked over this period by analysing the evolution of the calibration slopes. In Fig. S3, the sensitivity values obtained from the sodium and potassium sensors over multiple days are presented. The data clearly shows that both sensors experience a slight decrease in sensitivity during the first two days of measurements. However, from approximately day 4 to day 25, the slope remains remarkably stable, with only minimal deviations observed (consider that the scale is rather small). Throughout this period, the sensitivity values consistently remained above approximately 50 mV per decade of ion activity, which is considered suitable for experiments requiring reliable and precise sensor performance. Despite this stability, a significant drop in sensitivity is observed on the final recorded day, 30 for sodium and day 40 for potassium sensors. This reduction is likely due to the gradual degradation or wear of the ion-selective membrane deposited on the SNG-C electrodes, which can affect the sensor's responsiveness. Even after this decline, the sensors may still be suitable for applications where high sensitivity is not critical, allowing their continued use in less demanding experimental setups. These findings highlight the durability of the sensors over extended periods while also indicating a practical lifespan after which sensor recalibration or replacement may be necessary.

3.3 Selectivity Na^+ and K^+ sensor assay

Assessing the selectivity of the sensor is essential to determine the extent to which the complex composition of blood serum may interfere with accurate sodium or potassium ion measurements. Human serum contains a broad range of biological compounds, including electrolytes such as glucose, urea, lactate, proteins, hormones, lipids and metabolic products, which together create a challenging analytical matrix.[60,61] These substances can potentially affect the sensor response, leading to inaccurate readings if not properly accounted for. Therefore, evaluating selectivity ensures that the sensor can reliably distinguish sodium and

potassium ions from other coexisting species, reinforcing the importance of using robust and well-validated techniques for real sample analysis.

Selectivity of the sensor was evaluated using a procedure previously described in the literature,[43] as it was detailed in section 2.6. Considering the intended application of these sensors in biomedical samples, typical interferents commonly found in such matrices were selected for the study.[62] The selectivity was assessed by calculating the so-called "selectivity potential", following the approach outlined in eqn (3).

$$K^{POT} = \exp\left(\frac{E_J^O - E_I^O}{RT} \cdot z_I \cdot F\right) \qquad (3)$$

here, E_J and E_I represent the potential values measured in the presence of the target analyte and the interfering species, respectively;[43] R is the universal gas constant (J mol^{-1} K^{-1}), T is the absolute temperature in Kelvin, z_I denotes the charge of the interfering ion, and F is the Faraday constant (C mol^{-1}).

According to IUPAC guidelines[63] if the logarithmic selectivity coefficients are less than one, the sensor can be considered fully selective for analyte ions in the presence of the tested interferents. The calculated logarithmic selectivity coefficients are collected in Table 2. Since all the obtained values are below one, following IUPAC criteria, the sensors exhibited selectivity for potassium and sodium ions, even in the presence of tested interferents and at the concentrations evaluated.

Furthermore, the potential recorded by the sodium and potassium sensor was plotted against varying concentrations of potential interfering substances to assess any impact on the sensor response. As shown in Fig. S4 and S5, the sensors fabricated exhibited no variations in signal, indicating that their performance remains stable even in the presence of interfering species. This behaviour confirms the high selectivity of the sensors, following the selectivity criteria defined by the IUPAC for potentiometric measurements. The high selectivity of the sensors toward their respective ions is attributed to the ionophores incorporated during the

Table 2 Logarithmic selective coefficients calculated for the potassium and sodium potentiometric sensors using the separate solutions method (SSM)

Potassium sensor		Sodium sensor	
Interferent	K^{POT}	Interferent	K^{POT}
Na^+	−3.92	K^+	−2.62
NH_4^+	−4.62	NH_4^+	−2.33
Li^+	−4.26	Li^+	−3.04
Ca^{2+}	−3.99	Ca^{2+}	−2.54
Mg^{2+}	−4.34	Mg^{2+}	−2.05
Glucose	−3.56	Glucose	−2.68
Urea	−3.85	Urea	−3.16
Albumin	−3.60	Albumin	−3.30
Phosphate	−3.15	Phosphate	−3.56

membrane fabrication (section 2.4), valinomycin for potassium[73] and 4-tertiarybutylalkylix arene tetraethyl tetraester tetraethyl acid (sodium ionophore X) for sodium.[74] These ionophores form specific complexes with their target ions, facilitating their transport through the membrane and enabling selective detection by the sensor.

Following the individual selectivity assessment, triplicate measurements were conducted using sodium and potassium standards in artificial interstitial fluid. This step was key, as sensors are intended for complex matrices containing multiple interferents simultaneously. To evaluate performance under realistic conditions, results were compared with those obtained in the absence of interferents. The potassium sensor demonstrated consistent performance across different matrices, with an average sensitivity of 47.93 mV/log a_{K^+} (standard deviation: 1.99 mV) and a coefficient of variation of 4.14% in artificial interstitial fluid. These values are comparable to those obtained with potassium standard solutions without interferents. Similarly, calibration for sodium yielded a mean sensitivity of 53.73 mV/log a_{Na^+} with a standard deviation of 0.0016 mV and a coefficient of variation of 2.92%. These results confirm that the sensor provides accurate and reliable responses under both ideal and complex conditions, due to mainly the ionophore incorporated in the cocktail membrane. Moreover, the selectivity study indicates that calibration for real sample analysis can be performed without adding interferents to the standards, simplifying the analytical procedure.

3.4 Analysis of real samples under batch mode

A blood sample collected from adult volunteers was used to obtain the human serum and plasma samples. The blood sample was analysed with a blood gas analyser at the hospital. A total of six samples were analysed using the proposed sensors. Three were human serum and the rest were human plasma, obtained as described in section 2.9.

In situ analysis of the blood samples using a standard blood gas analyser allows for comparison with the results obtained using the proposed electrochemical system. This allowed for a direct comparison between the concentrations of sodium and potassium obtained with the proposed electrochemical sensor system and those measured by a standard clinical method. The close agreement between both sets of results confirmed the reliability and applicability of the developed platform for real biological samples. Additionally, the use of untreated serum in the analysis further demonstrates the robustness of the system in complex matrices without the need for sample pre-treatment.

To evaluate the practical applicability of the sensor, measurements were performed using untreated human serum and plasma, under discontinuous operation. As a first step, the analysis was focused on sodium determination. The sodium concentration in the selected biomedical samples, stablished by the blood gas analyser, was 138 mM. Sodium sensor recorded a potential of 0.378 V, which according to

the calibration curve, corresponds to an activity equivalent to a concentration of 136 ± 4.68 mM (n = 4). This result closely matches the reference value. To statistically validate the sensor performance in batch mode, a Student's t-test was carried out at a 95% confidence level. The calculated t value was 1.36, which is lower than the tabulated value of 3.18 for n = 4. Since $t_{calculated} < t_{tabulated}$, no statistically significant differences were observed, confirming the accuracy of the sensor for sodium detection in biomedical samples.

In the case of potassium sensor, the concentration in the real sample, by the blood gas analyser, was 4.6 mM. The recorded potential by the sensor was converted, using the corresponding calibration curve, into a concentration of 4.2 ± 0.36 mM (n = 4). The close agreement between both values suggests that the sensor provides reliable measurements for potassium. To verify these results, as in the previous experiment, another Student's t-test was applied. The calculated value was 1.92, which is lower than the tabulated value of 3.18 for n = 4. As previously explained, if $t_{calculated} < t_{tabulated}$, no statistically significant differences are observed. Thus, these findings expose the successful validation of the sensors.
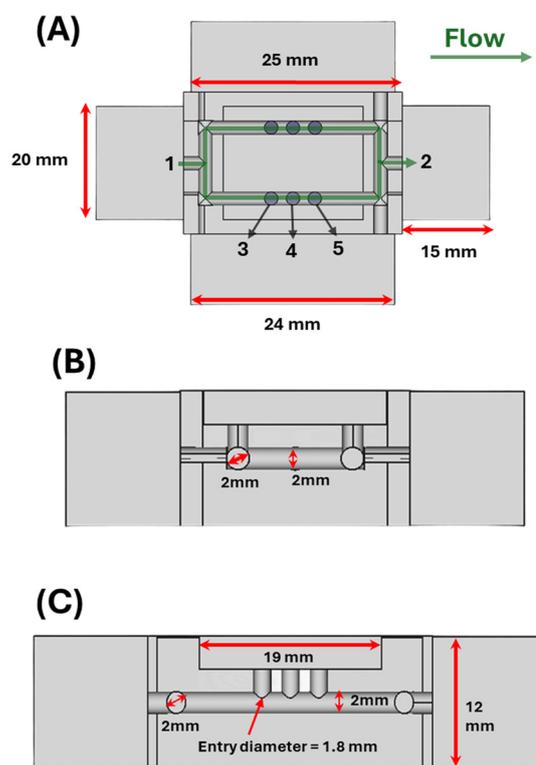

Fig. 4 Microfluidic cell design representations: (A) isometric view of the complete microfluidic cell, showing the general geometry and layout cut along plane Z. Green arrows indicate the sample flow, with 1 and 2 marking the sample inlet and outlet, respectively, and 3–5 indicating the openings for the working and reference electrodes. (B) Isometric view with a sectional cut along plane Y, revealing internal structures and channel configurations. (C) Lateral (side) view with a sectional cut along plane X, providing additional insight into internal flow paths and vertical arrangement of the microchannels.

3.5 Simultaneous detection of sodium and potassium in untreated human serum and plasma using continuous flow mode

The subsequent step involved testing the sensor for sodium and potassium ions in continuous mode to evaluate their suitability for real-time monitoring of these electrolytes in untreated human serum and plasma. A three-dimensional microfluidic cell was designed and fabricated *via* 3D printing to accommodate the specific dimensions of the SNG-C electrodes while minimizing the sample volume required (Fig. 4). The microfluidic cell was designed with two separate channels, one dedicated to the sodium sensors and the other to the potassium sensors. The cell includes an inlet for the introduction of sample or standard solutions and an outlet for their removal. To facilitate controlled flow, PTFE tubing was connected to both the inlet and the outlet, allowing precise and reproducible delivery of solutions through the respective channels. This configuration enables the simultaneous and independent measurement of sodium and potassium in a single microfluidic device. As indicated in section 2.8, PETG was selected as the material for fabricating the microfluidic cell. In previous work, our group has used other filaments, such as polylactic acid (PLA) and acrylonitrile butadiene styrene (ABS). While PLA is inexpensive and easy to print, it tends to react with the sample medium and, being biodegradable, may result in cells that are easily altered during use. ABS, on the other hand, was not selected due to potential safety risks, as printing ABS produces fumes that can be toxic for users without adequate safety precautions. For these reasons, PETG was chosen for its combination of biocompatibility, mechanical strength, and chemical inertness. Moreover, recent studies have confirmed that PETG is non-cytotoxic and complies with biocompatibility standards ISO 10993-5:2009 and ISO 10993-12:2021, making it suitable for biomedical applications.[75–77]

Calibrations were performed using several standard solutions with different concentrations of these ions, showing clear and consistent simultaneous responses for these ions. As illustrated in Fig. 5, the signal obtained by the sensors exhibits linearity with correlation coefficients (R^2) above 0.99 for both ions. It is noteworthy to mention that the sensitivities measured in continuous flow mode (0.4 mL min^{-1}) are usually lower than those obtained under batch conditions, likely due to reduced interaction time between the sensor surfaces and the analytical solutions.[64] These findings confirm the effectiveness of the custom-designed microfluidic cell and validate the combined application of sodium and potassium sensors for continuous, simultaneous ion monitoring in aqueous samples.

Finally, the developed sensors and microfluidic cells were applied in the simultaneous and continuous detection of sodium and potassium in untreated human serum and plasma. In total, two real biological samples were analysed: one plasma and one serum sample. Before performing the measurements under continuous flow conditions, the concentrations of sodium and potassium in each sample were determined using a commercial blood gas analyser. The obtained reference values were 4 mM for potassium and 137 mM for sodium. For the continuous flow measurements, each sample was introduced through PTFE tubing using a peristaltic pump, allowing the solution to pass into the microfluidic cell and come into direct contact with the ion-selective chemical sensors (Fig. 6). Under these conditions, the
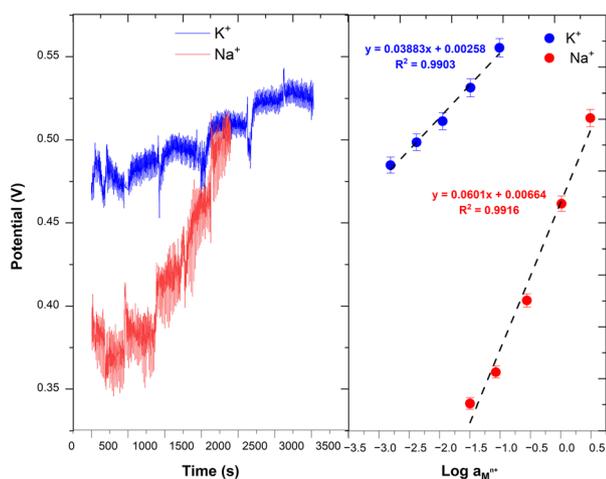
Fig. 5 Chronopotentiometric results and calibration curves under continuous flow conditions. The plot shows the electrochemical response of the sensors, along with the calibrated lines used to assess the linearity and sensitivity of the system during sustained operation. The flow speed applied was 0.4 mL min^{-1}.
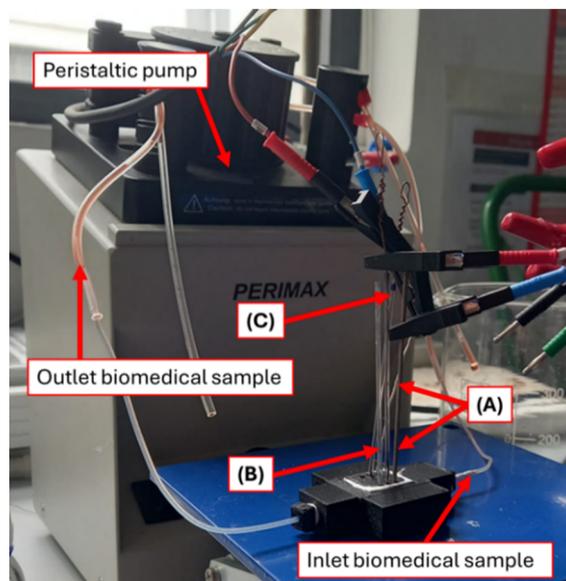
Fig. 6 Diagram of the measurement system in continuous mode. (A) Pseudo-reference electrode prepared in the laboratory; (B) sodium potentiometric sensor (working electrode); and (C) potassium potentiometric sensor (working electrode).

Table 3 Comparison of sodium and potassium concentrations in untreated serum and plasma samples obtained using the developed sensors, simultaneously and in continuous flow, and the reference method (blood gas analyser), including relative errors

Sample	[Na$^+$] BGA (mM)	[Na$^+$] ISE (mM)	Error (%)	[K$^+$] BGA (mM)	[K$^+$] ISE (mM)	Error (%)
S1	137	134	4.8	4	3.9	2.19
S2		133.7	3.75		3.85	2.31
S3		132.4	4.25		4.17	3.36
P1	135.74	133	4.88	4.06	3.9	2.92
P2		133.2	3.5		4.14	2.77
P3		141	3.75		4.15	2.92

S1: serum sample 1; S2: serum sample 2; S3: serum sample 3; P1: plasma sample 1; P2: plasma sample 2; P2: plasma sample 2; BGA: blood gas analyser (reference technique); ISE: ion-selective electrodes for Na$^+$ and K$^+$ proposed in this work.

potential generated by the interaction between the sensors and the sample was recorded. Using the calibration curves previously established and shown in Fig. 5, the logarithm of the ion activity was determined from the measured potential and subsequently converted into molar concentration. In this case, one human serum and plasma samples were obtained from a healthy volunteer. From this biological samples, a total of three serum aliquots and three plasma aliquots were analysed in this study in order to evaluate the performance of the developed chemical sensors under realistic biomedical conditions. All the samples were obtained from the same healthy volunteer, ensuring consistency in the biological matrix and electrolyte content. A standard blood gas analyser served as the reference method due to its widespread clinical acceptance and proven accuracy in measuring electrolyte levels in biological fluids.

Following this initial referencing, the same samples were subjected to analysis using the proposed chemical sensors under continuous flow conditions, without any prior sample treatment. This approach was designed to replicate real-time, in-line monitoring scenarios and to assess the capability of the sensors to operate effectively within complex biological matrices.

The experimental results obtained from the sensor-based measurements are summarized and compared to the reference values in Table 3. As illustrated in this table, the sodium and potassium concentrations measured using the developed sensors are in excellent agreement with those obtained from the reference method. Importantly, the relative errors observed in all cases were below 5%, which confirms both the accuracy and the reliability of the sensors when applied to untreated, real biological samples.

Not only do these findings highlight the high precision and reproducibility of the proposed sensors, but they also demonstrate their suitability for simultaneous, real-time detection of sodium and potassium ions in complex fluids such as serum and plasma. The ability to perform continuous monitoring without any pre-treatment of the samples represents a significant advantage for potential clinical and point-of-care applications, where rapid and accurate electrolyte analysis is critical for effective patient management.

Conclusions

The potentiometric sensors developed for the determination of sodium (Na$^+$) and potassium (K$^+$) ions have demonstrated excellent analytical performance under the conditions evaluated in this study. Both sensors responded accurately and reproducibly across a wide concentration range, including values corresponding to the lowest and highest physiological levels typically found in human blood and plasma, the sensors showed linear ranges of 38–4400 and 0.31–314 mM for sodium and potassium, respectively. The LOD and LOQ were 0.28/0.31 mM and 0.38/0.64 mM, respectively, while the sensitivities were 58 ± 0.5 and 54 ± 0.2 mV per decade. This effective determination within clinically relevant ranges represents a significant advancement in the design of sensors for biomedical applications. The sensor performance has been supported by sensitivity, detection limit, response time, and reproducibility, all of which showed acceptable values comparable to those obtained with alternative methodologies. Furthermore, their high selectivity for Na$^+$ and K$^+$ ions, even in the presence of common interfering species found in biological matrices, confirms their suitability for real-world applications. Notably, the simultaneous use of both sensors for the determination of sodium and potassium in untreated complex samples such as human plasma and serum proved to be feasible and effective. The results obtained were in good agreement with those obtained from the technique routinely employed in hospitals, reinforcing the potential of these devices as practical tools in clinical and diagnostic use. Moreover, these sensors present a very low cost compared to other approaches, such as laser-induced graphene-based methods, which can exceed 25€ per unit,[34] while our chemical sensors can be fabricated for less than 2€. Consequently, these sensors represent a promising alternative for the rapid, sensitive, and selective electrochemical analysis of electrolytes in biological fluids, with possible applications in clinical laboratories and point-of-care settings.

Author contributions

Á. J. S.-C.: conceptualization, software, validation, visualization, writing – original draft.; J. J. G.-G.:

conceptualization, resources, data curation, writing – original draft, funding acquisition.; D. B.-M.: conceptualization, data curation, writing – review and editing, supervision, project administration.; Á. C.-H.: methodology, software, validation, formal analysis, investigation.; M. J.-R.: methodology, validation, formal analysis, investigation.; V. G.-R.: methodology, validation, formal analysis, investigation.; L. C.-A.: resources, data curation, writing – review and editing, project administration, funding acquisition.; J. M. P.-S.: data curation, writing – review and editing, supervision, project administration, funding acquisition.

Conflicts of interest

The authors declare no conflicts of interest.

Ethical statement

All the studies implying research work applied to biological samples (human blood, plasma, and/or serum) were conducted in accordance with the Declaration of Helsinki, and the aforementioned projects and, consequently, the present study, in accordance with the Spanish regulation 'Real Decreto 1090/2015, de 4 de diciembre, por el que se regulan los ensayos clínicos con medicamentos, los Comités de Ética de la Investigación con medicamentos y el Registro Español de Estudios Clínicos', was approved by the Research Ethics Committee of Cadiz (Spain), on May 12, 2023, registry/protocol number 15.23. The resolution stated that the aforementioned projects, involving human samples, are viable, that they present sufficient methodological rigor, that the evaluation of economic costs are correct, and that with respect to the ethical aspects, the projects meet the necessary requirements of suitability of the protocol in relation to the objectives of the study.

Informed consent

All experiments were performed in accordance with the Guidelines of "Real Decreto 1090/2015, de 4 de diciembre, por el que se regulan los ensayos clínicos con medicamentos, los Comités de Ética de la Investigación con medicamentos y el Registro Español de Estudios Clínicos", and Experiments were approved by the Research Ethics Committee of Cadiz (Spain), on May 12, 2023, registry/protocol number 15.23 at University of Cadiz. Informed consents were obtained from human participants of this study.

Data availability

The data used to support the findings of this study are available from the corresponding author upon request.

Supplementary information (SI) is available. See DOI: https://doi.org/10.1039/d6lc00117c.

Notes and references

1 H. Haft and L. Allen, Primary Care and Public Health - Both Essential for National Health Security and Population Health, *J. Am. Board Fam. Med.*, 2024, **37**, S8–S11, DOI: 10.3122/jabfm.2023.230377R1.

2 K. C. Stange, W. L. Miller and R. S. Etz, The Role of Primary Care in Improving Population Health, *Milbank Q.*, 2023, **101**, 795–840, DOI: 10.1111/1468-0009.12638.

3 T. Oostrom, L. Einav and A. Finkelstein, Outpatient Office Wait Times and Quality of Care for Medicaid Patients, *Health Aff.*, 2017, **36**, 826–832, DOI: 10.1377/hlthaff.2016.1478.

4 A. X. G. P. Pereira and C. Dias-Ferreira, Healthcare Waste from Clinical Analysis Laboratories in São Tomé and Príncipe – Current State and Constrains in the Framework of Least Developed Countries, *Sustainable Chem. Pharm.*, 2023, **36**, 101318, DOI: 10.1016/j.scp.2023.101318.

5 M. Brommeyer, M. Whittaker, M. Mackay, F. Ng and Z. Liang, Building Health Service Management Workforce Capacity in the Era of Health Informatics and Digital Health – A Scoping Review, *Int. J. Med. Inform.*, 2023, **169**, 104909, DOI: 10.1016/j.ijmedinf.2022.104909.

6 M. R. Cowie, J. Bax, N. Bruining, J. G. F. Cleland, F. Koehler, M. Malik, F. Pinto, E. Van Der Velde and P. Vardas, E-Health: A Position Statement of the European Society of Cardiology, *Eur. Heart J.*, 2016, **37**, 63–66, DOI: 10.1093/eurheartj/ehv416.

7 R. R. Z. Tarpani and A. Gallego-Schmid, Environmental Impacts of a Digital Health and Well-Being Service in Elderly Living Schemes, *Clean. Environ. Syst.*, 2024, **12**, 100161, DOI: 10.1016/j.cesys.2023.100161.

8 A. Khan, E. DeVoe and S. Andreescu, Carbon-Based Electrochemical Biosensors as Diagnostic Platforms for Connected Decentralized Healthcare, *Sens. Diagn.*, 2023, **2**, 529–558, DOI: 10.1039/d2sd00226d.

9 J. Shlisky, R. Mandlik, S. Askari, S. Abrams, J. M. Belizan, M. W. Bourassa, G. Cormick, A. Driller-Colangelo, F. Gomes and A. Khadilkar, *et al.*, Calcium Deficiency Worldwide: Prevalence of Inadequate Intakes and Associated Health Outcomes, *Ann. N. Y. Acad. Sci.*, 2022, **1512**, 10–28, DOI: 10.1111/nyas.14758.

10 M. Barbagallo, N. Veronese and L. J. Dominguez, Magnesium in Aging, Health and Diseases, *Nutrients*, 2021, **13**, 1–20, DOI: 10.3390/nu13020463.

11 X. Li, Y. Yang, B. Zhang, X. Lin, X. Fu, Y. An, Y. Zou, J. X. Wang, Z. Wang and T. Yu, Lactate Metabolism in Human Health and Disease, *Signal Transduction Targeted Ther.*, 2022, **7**, 305, DOI: 10.1038/s41392-022-01151-3.

12 F. Arduini, L. Micheli, D. Moscone, G. Palleschi, S. Piermarini, F. Ricci and G. Volpe, Electrochemical Biosensors Based on Nanomodified Screen-Printed Electrodes: Recent Applications in Clinical Analysis, *TrAC, Trends Anal. Chem.*, 2016, **79**, 114–126, DOI: 10.1016/j.trac.2016.01.032.

13 M. McCaul, A. Porter, R. Barrett, P. White, F. Stroiescu, G. Wallace and D. Diamond, Wearable Platform for Real-Time Monitoring of Sodium in Sweat, *ChemPhysChem*, 2018, **19**, 1531–1536, DOI: 10.1002/cphc.201701312.

14 S. Yılmaz, H. B. Uysal, M. Avcil, M. Yılmaz, B. Dağlı, M. Bakış and I. K. Ömürlü, Comparison of Different Methods for Measurement of Electrolytes in Patients Admitted to the Intensive Care Unit, *Saudi Med. J.*, 2016, **37**, 262–267, DOI: 10.15537/smj.2016.3.13539.

15 F. Miller, J. Murray, A. Budhota, T. Harake, A. Steig, D. Whittaker, S. Gupta, R. Sivaprakasam and D. Kuraguntla, Evaluation of a Wearable Biosensor to Monitor Potassium Imbalance in Patients Receiving Hemodialysis, *Sens. Biosensing Res.*, 2023, **40**, 100561, DOI: 10.1016/j.sbsr.2023.100561.

16 M. O'Donnell, A. Mente and S. Yusuf, Sodium Intake and Cardiovascular Health, *Circ. Res.*, 2015, **116**, 1046–1057, DOI: 10.1161/CIRCRESAHA.116.303771.

17 C. M. Weaver, Potassium and Health, *Adv. Nutr.*, 2013, **4**, 368S–377S, DOI: 10.3945/an.112.003533.

18 H. T. Stelfox, S. B. Ahmed, F. Khandwala, D. Zygun, R. Shahpori and K. Laupland, The Epidemiology of Intensive Care Unit-Acquired Hyponatraemia and Hypernatraemia in Medical-Surgical Intensive Care Units, *Critical Care*, 2008, **12**, 6, DOI: 10.1186/cc7162.

19 V. Abate, A. Vergatti, N. Altavilla, F. Garofano, A. S. Salcuni, D. Rendina, G. De Filippo, F. Vescini and L. D'Elia, Potassium Intake and Bone Health: A Narrative Review, *Nutrients*, 2024, **16**, 3016, DOI: 10.3390/nu16173016.

20 D. Deriaz, N. Maes, P. Kolh and J. M. Krzesinski, Sodium and Potassium Intake: A New Statistical Model to Test Their Effects on Health Outcomes, *Kidney Int. Rep.*, 2020, **5**, 2403, DOI: 10.1016/j.ekir.2020.09.017.

21 P. K. Whelton, Sodium, Potassium, Blood Pressure, and Cardiovascular Disease in Humans, *Curr. Hypertens. Rep.*, 2014, **16**, 465, DOI: 10.1007/s11906-014-0465-5.

22 P. T. Nguyen, C. Deisl, M. Fine, T. S. Tippetts, E. Uchikawa, B. X. Chen and B. Levine, Structural Basis for Gating Mechanism of the Human Sodium-Potassium Pump, *Nat. Commun.*, 2022, **13**, 5293, DOI: 10.1038/s41467-022-32990-x.

23 R. Clough, C. F. Harrington, S. J. Hill, Y. Madrid and J. F. Tyson, Atomic spectrometry update: review of advances in elemental speciation, *J. Anal. At. Spectrom.*, 2023, **38**, 1339–1371, DOI: 10.1039/D3JA90022C.

24 R. Alvim García, C. Pereira Vanelli, O. S. Pereira Junior and J. O. do Amaral Corrêa, Comparative analysis for strength serum sodium and potassium in three different methods: Flame photometry, ion-selective electrode (ISE) and colorimetric enzymatic, *J. Clin. Lab. Anal.*, 2018, **32**(9), e22594, DOI: 10.1002/jcla.22594.

25 A. Taylor, N. Barlow, M. P. Day, S. Hill, M. Patriarca and M. White, Atomic spectrometry update: review of advances in the analysis of clinical and biological materials, foods and beverages, *J. Anal. At. Spectrom.*, 2016, **31**, 554–596, DOI: 10.1039/C6JA90005D.

26 P. J. Parsons and F. Barbosa, Atomic spectrometry and trends in clinical laboratory medicine, *Spectrochim. Acta, Part B*, 2007, **62**, 992–1003, DOI: 10.1016/j.sab.2007.03.007.

27 R. Thomas, *Practical Guide to ICP-MS: A Tutorial for Beginners*, CRC Press, Boca Raton, FL, USA, 3rd edn, 2013.

28 I. Sbai El Otmani, A. Amine and A. Dahmani, Comparative Evaluation of Sodium and Potassium Measurements by Flame Photometer and by Direct ISE Methods, *J. Chem. Pharm. Res.*, 2015, **7**(8), 862–867.

29 N. Fogh-Andersen and P. D. Wimberley, Determination of sodium and potassium with ion-selective electrodes, *Clin. Chem.*, 1984, **30**(4), 639–642, DOI: 10.1093/clinchem/30.4.639.

30 M. Cuartero and E. Bakker, Recent Advances in Ion-Selective Electrodes and Potentiometric Sensors, *Anal. Chim. Acta*, 2022, **1195**, 339422, DOI: 10.1016/j.aca.2022.339422.

31 C. Tang, W. Lin, Z. Du and X. He, Review of progresses on clinical applications of ion selective electrodes for electrolytic ion tests: from conventional ISEs to graphene-based ISEs, *Anal. Lett.*, 2016, **49**(14), 2137–2152, DOI: 10.1080/00032719.2016.1169560.

32 R. Paulauskas, N. Striūgas, M. Sadeckas, P. Sommersacher, S. Retschitzegger and N. Kienzl, Online Determination of Potassium and Sodium Release Behaviour during Single Particle Biomass Combustion by FES and ICP-MS, *Sci. Total Environ.*, 2020, **746**, 141162, DOI: 10.1016/j.scitotenv.2020.141162.

33 H. Liu, Z. Gu, Y. Liu, X. Xiao and G. Xiu, Validation of the Application of Solid Contact Ion-Selective Electrode for Off-Body Sweat Ion Monitoring, *Biosensors*, 2022, **12**, 12040229, DOI: 10.3390/bios12040229.

34 A. Esquerra-Zwiers, A. Vroom, D. Geddes and C. T. Lai, Use of a Portable Point-of-Care Instrumentation to Measure Human Milk Sodium and Potassium Concentrations, *Breastfeed. Med.*, 2022, **17**, 46–51, DOI: 10.1089/bfm.2021.0046.

35 H. Zhang, L. Sun, C. Song, Y. Liu, X. Xuan, F. Wang, J. Zhong and L. Sun, Integrated Solid-State Wearable Sweat Sensor System for Sodium and Potassium Ion Concentration

Detection, *Sens. Rev.*, 2022, **42**, 76–88, DOI: 10.1108/SR-03-2021-0081.

36 M. Alqarni, A portable paper-based sensor for simultaneous determination of sodium and potassium ions in the human plasma matrix, *Anal. Methods*, 2025, **17**, 3499–3508, DOI: 10.1039/D5AY00234F.

37 S. Farahani, K. A. McCracken, H. N. Medley and J. G. Bell, Fully 3D-printed solid-contact potentiometric sensor for sodium determination, *Biosens. Bioelectron.*, 2025, **289**, 117866, DOI: 10.1016/j.bios.2025.117866.

38 R. Ali, R. Almousa, S. M. Aly and S. M. Saleh, Nanoscale potassium sensing based on valinomycin-anchored fluorescent gold nanoclusters, *Microchim. Acta*, 2024, **191**, 299, DOI: 10.1007/s00604-024-06392-3.

39 A. Ghoorchian, M. Kamalabadi, M. Moradi, T. Madrakian, A. Afkhami, H. Bagheri, M. Ahmadi and H. Khoshsafar, Wearable Potentiometric Sensor Based on $Na_{0.44}MnO_2$ for Non-invasive Monitoring of Sodium Ions in Sweat, *Anal. Chem.*, 2022, **94**(4), 2263–2270, DOI: 10.1021/acs.analchem.1c04960.

40 S.-K. Cho and W.-J. Cho, Highly Sensitive and Selective Sodium Ion Sensor Based on Silicon Nanowire Dual Gate Field-Effect Transistor, *Sensors*, 2021, **21**, 4213, DOI: 10.3390/s21124213.

41 A. E. Oseyemi, A. Zabihihesari, S. Jafargholinejad and P. Rezai, Electrochemical microfluidic sensor with sodium ion-imprinted polymer membrane for sensitive and specific detection of sodium in water, *Microchim. Acta*, 2025, **192**(8), 520, DOI: 10.1007/s00604-025-07363-y.

42 J. J. García-Guzmán, Á. J. Sainz-Calvo, A. Sierra-Padilla, D. Bellido-Milla, L. Cubillana-Aguilera and J. M. Palacios-Santander, Simple and Cost-Effective pH and T Sensors from Top to Bottom: New Chemical Probes Based on Sonogel-Carbon Transducers for Plasma Analyses, *Talanta*, 2024, **270**, 125603, DOI: 10.1016/j.talanta.2023.125603.

43 Á. J. Sainz-Calvo, A. Sierra-Padilla, D. Bellido-Milla, L. Cubillana-Aguilera, J. J. García-Guzmán and J. M. Palacios-Santander, Fast, Economic, and Improved Nanostructured Polymeric pH Sensor for Agrifood Analysis, *Chemosensors*, 2025, **13**, 63, DOI: 10.3390/chemosensors13020063.

44 M. del M. Cordero-Rando, J. L. Hidalgo-Hidalgo de Cisneros, E. Blanco and I. Naranjo-Rodríguez, The Sonogel-Carbon Electrode as a Sol-Gel Graphite-Based Electrode, *Anal. Chem.*, 2002, **74**, 2423–2427, DOI: 10.1021/ac010782u.

45 L. M. Cubillana-Aguilera, J. M. Palacios-Santander, I. Naranjo-Rodríguez and J. L. Hidalgo-Hidalgo-De-Cisneros, Study of the Influence of the Graphite Powder Particle Size on the Structure of the Sonogel-Carbon Materials, *J. Sol-Gel Sci. Technol.*, 2006, **40**, 55–64, DOI: 10.1007/s10971-006-9151-7.

46 F. Valentini, A. Amine, S. Orlanducci, M. L. Terranova and G. Palleschi, Carbon Nanotube Purification: Preparation and Characterization of Carbon Nanotube Paste Electrodes, *Anal. Chem.*, 2003, **75**, 5413–5421, DOI: 10.1021/ac0300237.

47 G. Matzeu, C. O'Quigley, E. McNamara, C. Zuliani, C. Fay, T. Glennon and D. Diamond, An Integrated Sensing and

Wireless Communications Platform for Sensing Sodium in Sweat, *Anal. Methods*, 2016, **8**, 64–71, DOI: 10.1039/c5ay02254a.

48 W. Gao, S. Emaminejad, H. Y. Y. Nyein, S. Challa, K. Chen, A. Peck, H. M. Fahad, H. Ota, H. Shiraki, D. Kiriya, D. H. Lien, G. A. Brooks, R. W. Davis and A. Javey, Fully Integrated Wearable Sensor Arrays for Multiplexed in Situ Perspiration Analysis, *Nature*, 2016, **529**, 509–514, DOI: 10.1038/nature16521.

49 E. Bakker, E. Pretsch and P. Bühlmann, Selectivity of Potentiometric Ion Sensors, *Anal. Chem.*, 2000, **72**, 1127–1133, DOI: 10.1021/ac991146n.

50 T. Guinovart, G. A. Crespo, F. X. Rius and F. J. Andrade, A Reference Electrode Based on Polyvinyl Butyral (PVB) Polymer for Decentralized Chemical Measurements, *Anal. Chim. Acta*, 2014, **821**, 72–80, DOI: 10.1016/j.aca.2014.02.028.

51 A. Ghoorchian, M. Kamalabadi, M. Moradi, T. Madrakian, A. Afkhami, H. Bagheri, M. Ahmadi and H. Khoshsafar, Wearable Potentiometric Sensor Based on Na0.44MnO2 for Non-Invasive Monitoring of Sodium Ions in Sweat, *Anal. Chem.*, 2022, **94**, 2263–2270, DOI: 10.1021/acs.analchem.1c04960.

52 H. R. Lim, Y. S. Kim, S. Kwon, M. Mahmood, Y. T. Kwon, Y. Lee, S. M. Lee and W. H. Yeo, Wireless, Flexible, Ion-Selective Electrode System for Selective and Repeatable Detection of Sodium, *Sensors*, 2020, **20**, 1–11, DOI: 10.3390/s20113297.

53 M. Alqarni, A Portable Paper-Based Sensor for Simultaneous Determination of Sodium and Potassium Ions in the Human Plasma Matrix, *Anal. Methods*, 2025, **17**, 3499–3508, DOI: 10.1039/d5ay00234f.

54 M. Parrilla, R. Cánovas, I. Jeerapan, F. J. Andrade and J. Wang, A Textile-Based Stretchable Multi-Ion Potentiometric Sensor, *Adv. Healthcare Mater.*, 2016, **5**, 996–1001, DOI: 10.1002/adhm.201600092.

55 M. Parrilla, M. Cuartero, S. Padrell Sánchez, M. Rajabi, N. Roxhed, F. Niklaus and G. A. Crespo, Wearable All-Solid-State Potentiometric Microneedle Patch for Intradermal Potassium Detection, *Anal. Chem.*, 2019, **91**, 1578–1586, DOI: 10.1021/acs.analchem.8b04877.

56 N. Lenar, R. Piech and B. Paczosa-Bator, Candle Soot-Smoked Electrodes as a Natural Superhydrophobic Material for Potentiometric Sensors, *Talanta*, 2025, **285**, 127389, DOI: 10.1016/j.talanta.2024.127389.

57 Q. Wang, Á. Molinero-Fernández, J.-R. Acosta-Motos, G. A. Crespo and M. Cuartero, Unveiling Potassium and Sodium Ion Dynamics in Living Plants with an In-Planta Potentiometric Microneedle Sensor, *ACS Sens.*, 2024, **9**(10), 5214–5223, DOI: 10.1021/acssensors.4c01352.

58 N. Ruecha, O. Chailapakul, K. Suzuki and D. Citterio, Fully Inkjet-Printed Paper-Based Potentiometric Ion-Sensing Devices, *Anal. Chem.*, 2017, **89**, 10608–10616, DOI: 10.1021/acs.analchem.7b03177.

59 *ISO 5725-1:1994*, Accuracy (Trueness and Precision) of Measurement Methods and Results—Part 1: General

Principles and Definitions, International Organization for Standardization, Geneva, Switzerland, 1994.

60 H. T. Stelfox, S. B. Ahmed, F. Khandwala, D. Zygun, R. Shahpori and K. Laupland, The Epidemiology of Intensive Care Unit-Acquired Hyponatraemia and Hypernatraemia in Medical-Surgical Intensive Care Units, *Critical Care*, 2008, **12**, 6, DOI: 10.1186/cc7162.

61 R. A. Sulaiman, P. J. Twomey and R. Gama, Mitigation and Detection of Spurious Potassium and Sodium Results, *Clin. Chim. Acta*, 2011, **412**, 1–6, DOI: 10.1016/j.cca.2010.08.028.

62 Y. İspirli Doğaç and M. Teke, Urease Immobilized Core–Shell Magnetic Fe[NiFe]O$_4$/Alginate and Fe$_3$O$_4$/Alginate Composite Beads with Improved Enzymatic Stability Properties: Removal of Artificial Blood Serum Urea, *J. Iran. Chem. Soc.*, 2021, **18**, 2637–2648, DOI: 10.1007/s13738-021-02219-7.

63 H. J. Park, J. H. Yoon, K. G. Lee and B. G. Choi, Potentiometric Performance of Flexible pH Sensor Based on Polyaniline Nanofiber Arrays, *Nano Convergence*, 2019, **6**, 9, DOI: 10.1186/s40580-019-0179-0.

64 J. J. García-Guzmán, J. M. Jiménez Heras, D. López-Iglesias, R. J. González-Álvarez, L. Cubillana-Aguilera, C. González Macías, J. J. Fernández Alba and J. M. Palacios-Santander, New spin coated multilayer lactate biosensor for acidosis monitoring in continuous flow assisted with an electrochemical pH probe, *Microchim. Acta*, 2024, **191**, 9, DOI: 10.1007/s00604-024-06602-y.

65 E. Zdrachek and E. Bakker, Ion-to-electron capacitance of single-walled carbon nanotube layers before and after ion-selective membrane deposition, *Microchim. Acta*, 2021, **188**, 112, DOI: 10.1007/s00604-021-04805-1.

66 P. Wang, *et al.*, A review of the carbon-based solid transducing layer for ion-selective electrodes, *Molecules*, 2023, **28**, 5503, DOI: 10.3390/molecules28145503.

67 G. A. Crespo, S. Macho and F. X. Rius, Ion-Selective Electrodes Using Carbon Nanotubes as Ion-to-Electron Transducers, *Anal. Chem.*, 2008, **80**, 1316–1322, DOI: 10.1021/ac071156l.

68 D. Rajendran, R. Ramalingame, A. Adiraju, H. Nouri and O. Kanoun, Role of solvent polarity on dispersion quality and stability of functionalized carbon nanotubes, *J. Compos. Sci.*, 2022, **6**, 26, DOI: 10.3390/jcs6010026.

69 A. Abu Yaya, A. Tekley, E. Annan and L. R. Jensen, Dispersion and functionalization of single-walled carbon nanotubes (SWCNTs) for nanocomposite applications, *Appl. Phys. A: Mater. Sci. Process.*, 2016, **122**, 19, DOI: 10.1007/s00339-015-9618-3.

70 P. S. Goh and A. F. Ismail, Effect of acid oxidation on the dispersion property of multi-walled carbon nanotubes, *AIP Conf. Proc.*, 2009, **1136**, 224–228, DOI: 10.1063/1.3160172.

71 C. Saltiel, S. Manickavasagam, M. P. Mengüc and R. Andrews, Light-scattering and dispersion behavior of multiwalled carbon nanotubes, *J. Opt. Soc. Am. A*, 2005, **22**, 1546–1554, DOI: 10.1364/JOSAA.22.001546.

72 Y. Y. Huang and E. M. Terentjev, Dispersion of carbon nanotubes: Mixing, sonication, stabilization, and composite properties, *Polymers*, 2012, **4**, 275–295, DOI: 10.3390/polym4010275.

73 E. E. Totu, A. M. Josceanu and A. K. Covington, Improved potassium-selective membrane using valinomycin as ionophore for ion-selective microdevices, *Mater. Sci. Eng., C*, 2001, **18**, 87–91, DOI: 10.1016/S0928-4931(01)00374-5.

74 D. E. Carden, D. Diamond and A. J. Miller, An improved Na$^+$-selective microelectrode for intracellular measurements in plant cells, *J. Exp. Bot.*, 2001, **52**, 1353–1359, DOI: 10.1093/jexbot/52.359.1353.

75 Á. J. Sainz-Calvo, A. Sierra-Padilla, D. Bellido-Milla, L. Blanco-Díaz, J. J. Fernández-Alba, C. González-Macías, J. J. García-Guzmán, J. M. Palacios-Santander and L. Cubillana-Aguilera, Advancement in continuous lactate determination in untreated human serum: multipolymer-based amperometric biosensor coupled with a low-cost 3D-printed microfluidic cell, *Microchim. Acta*, 2026, **193**, 48, DOI: 10.1007/s00604-025-07771-0.

76 U. T. Strähle, N. Pütz and M. Hannig, A coating machine for coating filaments with bioactive nanomaterials for extrusion 3D printing, *Heliyon*, 2024, **10**, e33223, DOI: 10.1016/j.heliyon.2024.e33223.

77 D. Pyka, J. J. Słowiński, A. Kurzawa, M. Roszak, M. Stachowicz, M. Kazimierczak, M. Stępczak and D. Grygier, Research on basic properties of polymers for fused deposition modelling technology, *Appl. Sci.*, 2024, **14**, 11151, DOI: 10.3390/app142311151.